Palestine Technical University Research Journal, 2020, 8(2), 131-142

Uniaxial Strain and Optical Properties of GaP Nanowires

Rezek Mohammad[1*]

رزق محمد[1*]

[1]Department of Applied Physics, Applied Science College, Palestine Technical University Kadoorie, Tulkarm, Palestine

[1]قسم الفيزياء التطبيقية ، كلية العلوم التطبيقية، جامعة فلسطين التقنية خضوري، طولكرم، فلسطين

Received: 01/03/2020 **Accepted: 03/06/2020** **Published: 01/12/2020**

Abstract: The optical properties for wurtzite (WZ) Bulk GaP and GaP nanowires (GaP-NWs) in hexagonal(circular), triangular and square cross sectional are investigated by using full potential linear augmented plane waves and local orbitals (FP-LAPW-LO) method based on density functional theory (DFT). The wurtzite nanowires are investigated with diameters limited to ~27 oA. The optical functionsε_1 (ω), ε_2 (ω), n(ω), k(ω), σ(ω) and R(ω) as a function of photon energy have been investigated for unstrained bulk WZ-GaP and WZ-GaP-NWs in the first part. Finally, the optical functions are investigated for WZ-GaP-NWs by applying uniaxial strain from -5% to +5%. The effect of cross-sectional variation in the area and shape of the NWs on the optical functions is clear when compared with bulk GaP. GaP-NWs kept real dielectric constant ε_1 (ω) positive and refractive index n(ω) close to vacuum value for a wider range of energy on the contrary of bulk GaP. It is found that the dielectric constants ε_1 (ω) are slightly increased from the unstrained GaP-NWs values with strain increases. A shift in the threshold energy for ε_2 (ω) toward higher energy as the strain changes from tensile to compressive. The refractive index n(ω) shows a small change when passing from compressive toward tensile strain. It is found that GaP-NWs could play a role in solar cells structure and high-speed electronic circuits.

Keywords: GaP Nanowire, Optical properties, Dielectric constant, Refractive index, First-principles, Solar Cell.

INTRODUCTION:

The optical properties of Semiconductor Nanowires (NWs) (high refractive index, light confinement, and uniform diameter) offer excellent base Nanoscale optical circuits (Chad Husko. et al, 2018; Xiaojie, 2015; Peidong, 2010; Xing, 2014; Habeom et al, 2017; Muskens et al, 2008; Muskens et al, 2009; Ochoa-Martínez et al, 2018). In (Chad Husko. et al, 2018) the authors stated that the direct band gap of few-layer phosphorene super celled with silicon demonstrates optical emission in the telecommunications 1550 nm window. Xiaojie, et al (2015), explained the use of nanocircuits in the study of neural circuits, and Muskens et al, (2008), shows fascinating progress in the field of III-V Nanowires solar cells because of the low cost and advanced techniques of fabrication. Ochoa-Martínez, et al, (2018), and his colleges concluded, the determination of the optical constants of III-V phosphide-based materials with the typical

* Corresponding author: esteteh@hotmail.com

doping levels and growth conditions applied in the fabrication of multi-junction solar cells is essential to improve the accuracy of the models used to predict the solar cell performance. A40% efficiency reached in solar cells by using multi-layer semiconductors (Yamaguchi et al, 2003; Kang et al, 2004). The Semiconductor NWs composition and orientation are controlling the electrical, magnetic, thermal and mechanical properties (Long et al, 2005; Zeng et al, 2000; Deyu Li et al, 2003; A'lvaro et al, 2007).

The physical shape of semiconductor NWs makes a huge mismatch in the refractive index between the NW and its surroundings. Semiconductor NWs with a smaller diameter compared to the wavelength of light, confine optical waves in the radial direction, while leading them along an axial direction (Tong et al, 2004; Tong et al, 2003). Because of this semi cylindrical structure, optical properties studies are impossible for a wide range of photon energy. As a result of the above, the full range energy-wave vector dispersion relation of the NW is controlled by structure and geometry. In previous works (Khordad et al, 2015; Yao, 2009; Vashaee et al, 2006; Gradeak et al, 2005), it is found that surface shape of the NWs controls their optical and electronic properties.

GaP-NWs have an energy gap in the visible range and nearly is nearly transparent in the range 0.53 to 4 μm (Borghesi et al, 1991). In addition to the electronic properties, GaP-NWs can be easily fabricated to be adopted in light-emitting diodes (LEDs) (McIntosh et al, 2011), solar cells (Vaisman et al, 2015; Jordan et al, 2013), field effect transistors (FETs) and a lot of applications (Mohammad et al, 2019; Lin et al, 2015; Sanatinia et al, 2012).

Almost all the applications on NWs composed of superlattices from different NW materials, the same effect noticed when using a substrate from different material to build the desired NW, this change in the bond length with respect to the bulk bond length in the same NW material, results in a contraction or an extraction in the bonds of the NW, this contraction or extraction studied in the present work by applying strain up to ± 5% for the hexagonal(circular), triangular and square cross-sectional shapes for the GaP-NWs.

Since optical properties rely on the internal electronic structures of nanomaterials, that's why studying optical properties of nanomaterials can give us an intense understanding of their structure (Hwang et al, 2014; Kumar et al, 2010; Kim et al, 2014; Allali et al, 2014; Logothetidis et al, 1994; Anani et al, 2008).

In the present work, the dielectric constant, refractive index, reflectivity, and conductivity of wurtzite GaP (WZ-GaP) NWs are investigated for namely, hexagonal, triangular, and rectangular cross sections. Additionally, mechanical strain effects on the above optical functions are examined for WZ-GaP-NWs which are stretched and compressed by the uniaxial strains up to 5%.

The Optical Properties of the unstrained and strained nanowires are carried out by first-principles calculations based on Density Functional Theory (DFT). The calculation method of GaP-NWs is presented in Sec. 2. The optical constants of the hexagonal, triangular and rectangular nanowires are presented and compared in Sec. 3. The strain effect on the optical constants of the GaP-NWs is examined in Sec. 4. The conclusions are summarized in Sec. 5.

Calculation Method and Optical Properties:

The optical properties of GaP-NWs in Wurtzite phase have been investigated using normalized wave functions for all the electrons in the NWs. The normalized wave functions are calculated by density functional theory as explained in our previous work (Mohammad et al, 2019). Since optical properties calculations require a dense mesh of distributed k points. The irreducible Brillouin zone is sampled with a sufficiently large number of 560 k-points for Bulk GaP-WZ, and 32 k-points for all the nanowires of this work using (3X3X12) Monkhorst Pack mesh.

The optical properties of the material can be derived from the complex dielectric function $\varepsilon(\omega) = \varepsilon_1(\omega) + i\,\varepsilon_2(\omega)$. The dielectric constant inversely related to the collum potential between electrons, holes and ions, which makes the material directly affected by the electromagnetic radiation. The real part of the dielectric function $\varepsilon_1(\omega)$ explains how the electromagnetic energy spared in the material. This function $\varepsilon_1(\omega)$ evaluated from the imaginary part of the dielectric function $\varepsilon_2(\omega)$ using Kramers-Kronig transformation. The imaginary part of the dielectric function $\varepsilon_2(\omega)$ corresponds to the photon absorbed in the material with energy $E(\omega) = \hbar\omega$. This function $\varepsilon_2(\omega)$ can be calculated from the momentum matrix elements between the occupied and unoccupied states using the following formula (Claudia et al, 2006):

$$\varepsilon_2(\omega) = \frac{e^2\,\hbar}{\pi m^2 \omega^2} \sum_{c,v} \int_{B\,Z} |M_{cv}(k)|^2 \delta[\omega_{cv}(k) - \omega] d^3k$$

where the integral is over the brillouin zone, $M_{cv}(k) = \langle u_{ck}|e\nabla|u_{vk}\rangle$ is the dipole matrix elements for direct transitions between valence and conduction states at the specific k points, e∇ is the polarisation vector of the electric field associated with the electromagnetic incident photon, u_ck and u_vk are the self-consistent wave functions for conduction and valence states at this particular k point, respectably, $\hbar\omega(k) = E_c(k) - E_v(k)$ is the excitation energy between the valence band and conduction band at this particular k point. The real part $\varepsilon_1(\omega)$ is extracted from the imaginary part $\varepsilon_2(\omega)$ by Kramers-kronig relation (Claudia et al, 2006):

$$\varepsilon_1(\omega) = 1 + \frac{2}{\pi} P \int_0^{\infty} \frac{\acute{\omega}\varepsilon_2(\acute{\omega})}{(\acute{\omega}^2) - \omega^2}\, d\acute{\omega}$$

where P is the principal value of the integral. The frequency dependent refractive index $n(\omega)$is calculated using both types of the dielectric constants by the following formula (Claudia A., et al, 2006):

$$n(\omega) = \left[\frac{\sqrt{\varepsilon_1(\omega)^2 + \varepsilon_2(\omega)^2}}{2} + \frac{\varepsilon_1(\omega)}{2}\right]^{1/2}$$

The frequency dependent imaginary part of the refractive index (extinction coefficient) $k(\omega)$ is calculated as follows (Claudia A., et al, 2006):

$$k(\omega) = \left[\frac{\sqrt{\varepsilon_1(\omega)^2 + \varepsilon_2(\omega)^2}}{2} - \frac{\varepsilon_1(\omega)}{2}\right]^{1/2}$$

Experimentally $n(\omega)$ and $k(\omega)$ are measured from the reflectivity coefficient $R(\omega)$ or Optical absorption coefficient $\alpha(\omega)$. The reflectivity can be found from dielectric constant as follows (Claudia A., et al, 2006):

$$R(\omega) = \frac{(n-1)^2 + k^2}{(n-1)^2 - k^2}$$

RESULTS AND DISCUSSION:

In the present work, three different cross-sectional shapes of NWs used in the calculation (Hexagonal, Triangular and square). The structure of each NW is explained in our previous work (Mohammad et al, 2019). The optical parameters: dielectric constants $\varepsilon_1(\omega), \varepsilon_2(\omega)$, refractive index $n(\omega)$, extinction coefficient $k(\omega)$, reflectivity $R(\omega)$, and the conductivity $\sigma(\omega)$, for bulk GaP in wurtzite phase (WZ-GaP) and all NWs were calculated for the range from 0 to 15 eV. The values for these parameters at important energy values are tabulated in **Table (1)**. $\varepsilon_1(0)$ values for all NWs are ascending as the volume (diameter) of the NW unit cell increase, these values gradually increasing from 1.191 for smallest NW to 4.910 for the biggest NW tending the present bulk calculated value 10.596. This calculated value is very close to experimental value 10.102 (Aspnes., 1983), and other theoretical calculations ranging from 7.31 to 11.1 (Moussa et al, 2015).

The NW diameter, surface shape and cross-sectional area to volume of the NW unit cell affect highly the optical parameters. The increase in these effects makes the valence electrons closer to the ions, which results in a bigger electrical energy. This can be seen in the $\varepsilon_1(0)$, $\varepsilon_1(\omega)_{max}$ and $\varepsilon_1(\omega)_{min}$values. **Fuigure. (1-a)** shows real dielectric function $\varepsilon_1(\omega)$ versus photon energy for calculated bulk GaP-WZ and selected NWs (Hex-1 to Hex-4, Rec-1 to Rec-2). The triangular NWs values are in the same range of the selected NWs. **Fuigure (1-a**) shows that $\varepsilon_1(\omega)$ is positive for photon energy less than 4 eV. This means that bulk GaP and GaP-NWs can store the photon energy inside the material in that range. For photon energy greater than 4 eV bulk GaP becomes very metallic and reflects the incoming photons, while GaP NWs $\varepsilon_1(\omega)$ are positive up to 5 eV and close to zero above that range, so they are not reflecting the incident photons in that range, which covers all the visible spectrum.

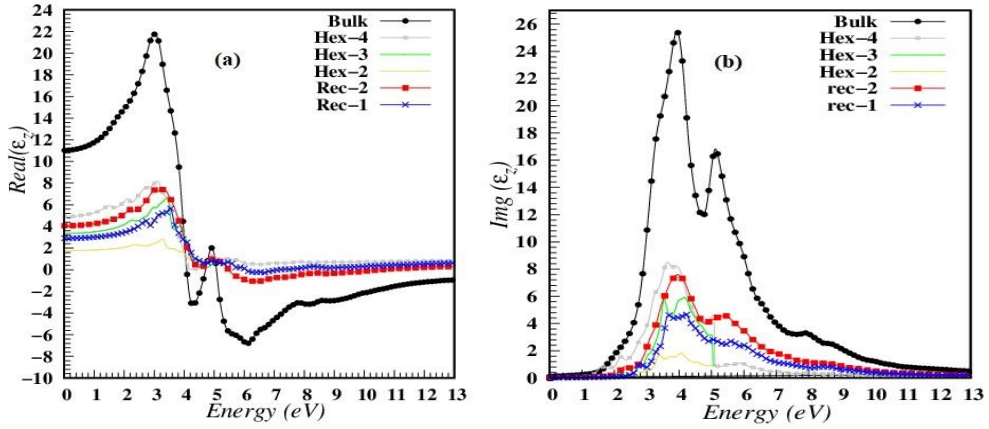

Figure (1-a) The variation of real dielectric constant $\varepsilon_1(\omega)$ for bulk GaP and GaP-NWs for Hex-2 to Hex-4, Rec-1 and Rec-2 in arbitrary units Versus photon energy (eV), (b) The variation of imaginary dielectric constant $\varepsilon_2(\omega)$ for bulk GaP and GaP-NWs for Hex-2 to Hex-4, Rec-1 and Rec-2 in arbitrary units Versus photon energy (eV).

The imaginary dielectric constant $\varepsilon_2(\omega)_{max}$values for NWs listed in table 1 are increasing by the same order toward the bulk calculated value of 25.422 which is very close to a theoretical calculated value of 26.580 (Aspnes et al, 1983). The $\varepsilon_2(\omega)$ threshold energy is inversely proportional to NW diameter. The threshold energy depends on the NWs energy gap, where the NW begins absorption of incident photons. The threshold energy decreases with the diameter increase. The smallest threshold energy for Hex-4 is 0.872 which is smaller than the experimental value 2.2 (Aspnes et al, 1983). The inconstancy between the NWs convergent value and the experimental value is related to the underestimating of the energy gap by first principle calculations. Fuigure.1-b shows the variation of imaginary dielectric constant $\varepsilon_2(\omega)$ for bulk GaP-WZ and selected NWs versus the energy of the photon.

Table (1) The dielectric constant at zero energy $\varepsilon_1(0)$, maximum values of $\varepsilon_1(\omega)_{max}$, $\varepsilon_2(\omega)_{max}$, $n(\omega)_{max}$, $k(\omega)_{max}$, $\sigma(\omega)$, $R(\omega)_{max}$ spectra and the energy values where the peaks occur, the threshold energy of $\varepsilon_2(\omega)_{max}$, and the minimum value for $\varepsilon_1(\omega)_{min}$ for GaP-NWs Hex-1-Hex-4, Tri-1-Tri-3 and Rec-1-Rec-3 with zero strain.

Parameter	Hex-1	Hex-2	Hex-3	Hex-4	Tri-1	Tri-2	Tri-3	Rec-1	Rec-2	Rec-3
$\varepsilon_1(0)$ (arb. unit)	1.191	1.779	3.360	4.910	2.486	2.874	3.329	2.906	4.060	3.755
$\varepsilon_1(\omega)_{max}$ (arb. unit)	1.681	2.824	6.629	8.178	5.488	5.377	5.629	5.707	7.419	6.659
Energy at $\varepsilon_1(\omega)_{max}$ eV	3.796	3.279	3.415	3.116	3.605	3.387	3.279	3.524	3.306	3.034
$\varepsilon_1(\omega)_{\min}$	0.830	0.493	-0.603	-1.531	0.378	-0.292	-0.607	-0.273	-1.091	-1.281
Energy at $\varepsilon_1(\omega)_{min}$ eV	4.857	6.544	6.136	6.327	5.646	6.299	6.245	6.653	6.190	6.353
$\varepsilon_2(\omega)_{max}$ (arb. unit)	0.680	1.808	5.905	8.509	4.609	5.202	5.512	4.728	7.592	8.660
Energy at $\varepsilon_2(\omega)_{max}$ eV	4.422	0.775	4.177	3.633	4.068	4.176	3.796	4.177	3.959	3.878
$\varepsilon_2(\omega)$ energy threshold (eV)	3.633	2.190	1.735	0.872	2.435	2.027	1.510	2.109	1.510	1.129
$n(0)$ (arb. unit)	1.092	1.334	1.833	2.216	1.577	1.695	1.825	1.705	2.015	1.938
$n(\omega)_{max}$ (arb. unit)	1.304	1.716	2.699	2.982	2.416	2.384	2.451	2.488	2.833	2.692
Energy at $n(\omega)_{max}$ eV	3.823	3.442	3.279	3.143	3.632	3.415	3.333	3.551	3.361	3.061
$k(\omega)_{max}$ (arb. unit)	0.309	0.692	1.508	1.870	1.265	1.407	1.464	1.298	1.700	1.930
Energy at $k(\omega)_{max}$ eV	4.449	4.395	4.258	4.095	4.340	4.286	4.095	4.258	4.204	4.122
$k(\omega)$energy threshold (eV)	3.783	2.381	2.231	1.455	2.871	2.462	1.871	2.626	2.163	1.523
$\sigma(\omega)_{max}$ $(\Omega^{-1}cm^{-2})$	0.366	0.889	2.982	3.896	2.341	2.564	2.887	2.397	2.674	3.647
Energy at $\sigma(\omega)_{max}$ eV	4.449	4.068	4.177	3.959	5.537	4.204	4.150	4.204	4.013	3.932
$\sigma(\omega)$ energy threshold (eV)	3.758	2.408	2.201	1.483	2.816	2.417	1.891	2.571	2.136	1.564
$R(0)$ (arb. unit)	0.002	0.002	0.086	0.143	0.050	0.067	0.085	0.068	0.113	0.102
$R(\omega)_{max}$ (arb. unit)	0.023	0.098	0.288	0.393	0.237	0.284	0.298	0.243	0.296	0.346
Energy at $R(\omega)_{max}$ (eV)	3.878	4.095	4.231	6.353	4.286	5.619	6.245	4.150	4.258	6.472

The refractive index at low photons energy denoted by n (0) in Table 1 is consistent with the relation n (0) =√ (ε_1 (0)) (Claudia et al, 2006). The maximum refractive index is found to increase with the diameter of the NW. Bulk GaP refractive index is found experimentally to be 3.178 (Aspnes et al, 1983), 3.321 (in the present work) and 3.28 (Moussa et al, 2015) in other theoretical works .

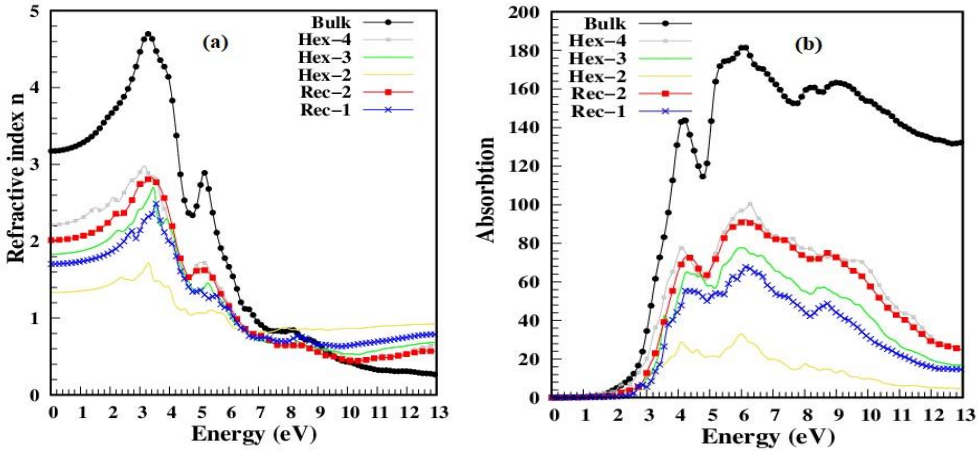

Figure (2-a) The variation of refractive-index n(ω) for bulk GaP and GaP-NWs for Hex-2 to Hex-4, Rec-1 and Rec-2 in arbitrary units Versus photon energy (eV), (b)The variation of absorption α(ω) for bulk GaP and GaP-NWs for Hex-1 to Hex-4, Rec-1 and Rec-2 in arbitrary units Versus photon energy (eV)

Figure (2-a) shows the refractive index variation versus the photon energy. The NWs refractive index variation is similar to the bulk variation. NWs have smaller refractive index for the energy of the photon less than 8 eV closer to the vacuum refractive index value depending on the diameter. The speed of the photons inside the NWs is faster along the NWs axis than the bulk. The extinction constant $k(\omega)$ is the imaginary part of the refractive index. From **Table-1** $k(\omega)_{max}$, photon energy where this value occurs and $k(\omega)$ threshold energy are all decreasing with NWs radius increase. **Figure (2-b**) shows the absorption of bulk GaP-WZ and selected NWs with respect to the photon's energy, it is clear from the Fuigure. 2 that larger surface areas NWs are closer to the bulk absorption. All NWs and bulk have the same peak at 3 eV. The conductivity is energy gap dependent. Maximum conductivity increases for all NWs with diameter increase, oppositely the maximum conductivity occurs at higher photon energy for smaller diameter. This can also be noticed from threshold energy of the conductivity for the three NWs structure shapes. The smaller the diameter the bigger the threshold energy is. The variation in reflectivity R (0) and maximum reflectivity R(ω) are very small and increases with the surface area of the NW, the photon energy at maximum reflectance also increase with diameter increase.

Stain and Optical Parameters:

In the present section, the optical parameters are recalculated under uniaxial strain, since the presented difference between the axial optical parameters and the radial ones are very small (Saadi., 2017), and the mismatch, superlattices occur along NWs axis, we limit our discussion to the optical parameters variation verses strain applied along the axial direction. From our previous work Mohammad et al, (2019), the unit cell volume and surface area for Hex-2, Tri-2 and Rec-2 NWs are almost equal. A comparison was made between the dielectric constants for the three NWs to show cross sectional shape effect. It was found that $\varepsilon_1(0)$ for Hex-2 becomes 2.068 under the maximum compressive strain (-5%) and 2.205 under maximum tensile strain (+5%), which means $\varepsilon_1(0)$ and n (0) are both increase with compressive and tensile strain for Hex-2 NW. Tri-2 NWs show the same trend for $\varepsilon_1(0)$ and n (0) as well. It becomes 3.772

for -5% strain and 4.298 for +5% strain. Oppositely we notice in Rec-2 that $\varepsilon_1(0)$ and n (0) decrease with compressive strain, $\varepsilon_1(0)$ reaches 3.772 for Rec-2 when strain -5%, and becomes 4.298 when strain reaches +5%. **Figure (3-a)** shows the variation of $\varepsilon_1(\omega)$ versus photon energy together with the calculated $\varepsilon_1(\omega)$ for the maximum limit strains ±5%. **Figure (3-a)** shows that NW has the same variation with a small shifting in the peaks position and always has a positive real dielectric constant

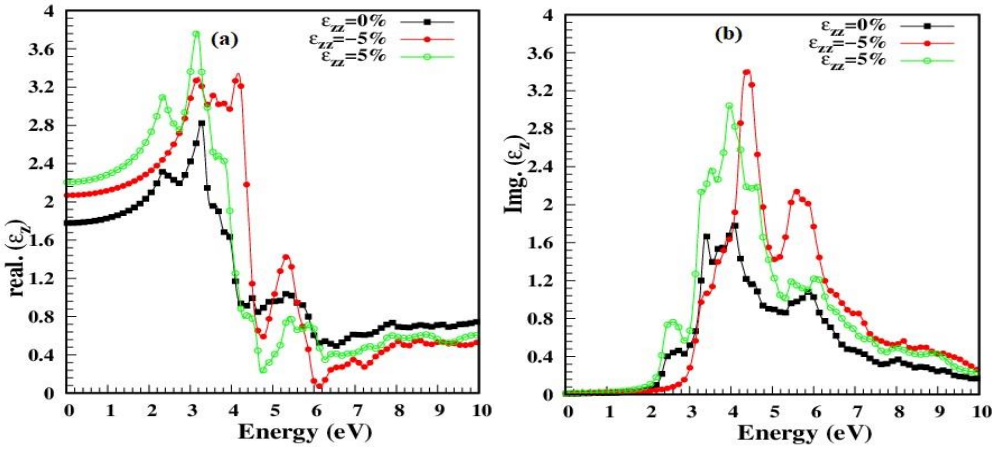

Figure (3-a): The variation of real dielectric function $\varepsilon_1(\omega)$ for GaP-NW Hex-2 at uniaxial strains -5%, 0 and +5% in arbitrary unit's verses photon energy(eV). (b): The variation of imaginary dielectric function $\varepsilon_2(\omega)$for GaP-NW Hex-2 at uniaxial strains -5%, 0 and +5% in arbitrary unit's verses photon energy(eV).

The imaginary dielectric function $\varepsilon_2(\omega)$ shows an increase in Hex-2 for both strains, $\varepsilon_2(\omega)_{max}$reaches 3.423 for maximum compressive strain, while reaches the value 3.044 for maximum tensile strain, **Fuigure. 3-b** shows the variation of $\varepsilon_2(\omega)$ versus photon energy for maximum strains ±5% and zero strain. The $\varepsilon_2(\omega)$ threshold energy for the NW defer according to the applied strain. In general, $\varepsilon_2(\omega)$ is bigger when both type of strains are greater than zero strain.

The same trend was noticed for Tri-2 NW, where $\varepsilon_2(\omega)$ reaches 5.746 for compressive strain and 5.943 for tensile strain.

Table (2) and **Table (3)** shows the calculated optical parameters for real and imaginary parts of the dielectric function, real and imaginary refractive index $n(\omega)$, $k(\omega)$, respectively, reflectance $R(\omega)$and conductivity $\sigma(\omega)$ at important photon energy.

CONCLUSION:

In the first stage of this work, the optical functions $\varepsilon_1(\omega), \varepsilon_2(\omega), n(\omega), k(\omega), \sigma(\omega)\ and\ R(\omega)$as a function of photon energy $E = \hbar\omega$ for bulk WZ-GaP phase in addition to the hexagonal, triangular and rectangular cross-sectional GaP-NWs with diameters ranging from $\sim 5\ A^o$ to $\sim 27\ A^o$ are studied by DFT-FP-LAPW-PBE calculations.

It is found that bulk GaP had a negative dielectric constant $\varepsilon_1(\omega)$for photons energy greater than 4 eV. That's make bulk GaP absorbent material for electromagnetic waves up to 4 eV. GaP-NWs have always a positive dielectric constant $\varepsilon_1(\omega)$. The smaller value of $\varepsilon_1(\omega)$in the NWs also indicate that incident photons pass through the NWs (transparent NWs), which make GaP-NWs a good candidate for solar cells cover.

It was found also that refractive index for GaP-NWs n(ω) in the visible range is smaller than bulk GaP, which allows incident photons to pass through the NWs in speed closer to the speed of light in vacuum, which makes this GaP-NWs a good candidate to high-speed electronic circuits.

In the second stage, the effects of the uniaxial mechanical strains on the optical parameters of GaP-NWs are investigated, the previous optical functions are recalculated for NWs under uniaxially and laterally stretched/compressed strains from -5% to +5%. All the strained GaP nanowires of this work show that the optical functions are very close to the NWs with zero strain, the maximum strain resulted in a change < 10% in the real dielectric constant, while the other parameters didn't exceed this value, it is also found that under this maximum strain the NWs are kept their transparency to incident photons.

Table(2):The dielectric constant at zero energy $\varepsilon_1(0)$, maximum values of $\varepsilon_1(\omega)_{max}$, $\varepsilon_2(\omega)_{max}$, $n(\omega)_{max}$, $k(\omega)_{max}$, $\sigma(\omega)$, $R(\omega)_{max}$ spectra and the energy values where the peaks occur, the threshold energy of $\varepsilon_2(\omega)_{max}$ and the minimum value for $\varepsilon_1(\omega)$ for Rec-1 GaP-NWs with stain along z direction.

Parameter	-5%	-4%	-3%	-2%	-1%	0%	1%	2%	3%	4%	5%
$\varepsilon_1(0)$ (arb. unit)	2.813	2.814	2.821	2.791	2.829	2.906	2.873	3.005	3.061	3.086	3.045
$\varepsilon_1(\omega)_{max}$ (arb. unit)	4.805	4.925	5.104	4.822	5.538	5.707	5.233	5.800	6.260	6.083	5.431
Energy at $\varepsilon_1(\omega)_{max}$ eV	3.143	3.496	3.523	3.551	3.551	3.524	3.197	3.143	3.143	3.088	2.925
$\varepsilon_1(\omega)_{min}$	-0.55	-0.56	-0.47	-0.37	-0.29	-0.27	-0.26	-0.32	-0.30	-0.27	-0.07
Energy at $\varepsilon_1(\omega)_{min}$ eV	6.435	6.272	6.326	6.353	6.408	6.653	6.680	6.381	6.381	4.313	6.435
$\varepsilon_2(\omega)_{max}$ (arb. unit)	5.017	4.902	4.733	4.517	4.464	4.728	4.562	5.351	5.409	5.499	5.043
Energy at $\varepsilon_2(\omega)_{max}$ eV	4.258	4.204	4.231	4.231	3.687	4.177	3.660	3.524	3.551	3.524	3.959
$\varepsilon_2(\omega)$ energy threshold (eV)	2.299	2.285	2.255	2.225	2.190	2.109	2.054	1.837	1.810	1.700	1.592
$n(0)$ (arb. unit)	1.677	1.678	1.680	1.671	1.682	1.705	1.695	1.734	1.750	1.757	1.745
$n(\omega)_{max}$ (arb. unit)	2.278	2.276	2.331	2.268	2.448	2.488	2.393	2.507	2.570	2.534	2.376
Energy at $n(\omega)_{max}$ eV	4.095	3.523	3.524	3.578	3.578	3.551	2.524	3.415	3.170	3.116	2.952
$k(\omega)_{max}$ (arb. unit)	1.248	1.252	1.227	1.203	1.188	1.298	1.238	1.439	1.469	1.454	1.428
Energy at $k(\omega)_{max}$ eV	4.340	6.191	4.285	4.313	4.367	4.258	4.177	4.258	4.231	4.122	4.014
$k(\omega)$ energy threshold (eV)	2.898	2.898	2.843	2.789	2.735	2.626	2.571	2.354	2.326	2.217	2.027
$\sigma(\omega)_{max}$ $(\Omega^{-1}cm^{-2})$	2.591	2.492	2.421	2.318	2.227	2.397	2.239	2.391	2.402	2.375	2.414
Energy at $\sigma(\omega)_{max}$ eV	4.286	4.204	4.231	4.258	4.231	4.204	4.122	4.068	4.123	4.041	3.959
$\sigma(\omega)$ energy threshold (eV)	2.762	2.762	2.734	2.707	2.653	2.571	2.544	2.326	2.299	2.205	2.012
$R(0)$ (arb. unit)	0.064	0.064	0.064	0.063	0.065	0.068	0.067	0.072	0.074	0.075	0.074
$R(\omega)_{max}$ (arb. unit)	0.276	0.279	0.264	0.248	0.235	0.243	0.231	0.279	0.289	0.283	0.272
Energy at $R(\omega)_{max}$ eV	6.272	6.245	6.299	6.353	6.408	4.258	4.15	4.286	4.286	4.204	4.104

Table(3):The dielectric constant at zero energy $\varepsilon_1(0)$, maximum values of $\varepsilon_1(\omega)_{max}, \varepsilon_2(\omega)_{max}, n(\omega)_{max}, k(\omega)_{max}, \sigma(\omega), R(\omega)_{max}$ spectra and the energy values where the peaks occur, the threshold energy of $\varepsilon_2(\omega)_{max}$ and the minimum value for $\varepsilon_1(\omega)$ for Rec-2 GaP NWs with stain along z direction.

Parameter	-5%	-4%	-3%	-2%	-1%	0%	1%	2%	3%	4%	5%
$\varepsilon_1(0)$ (arb. unit)	3.772	3.771	3.813	3.851	3.881	4.060	3.900	3.948	4.039	4.173	4.298
$\varepsilon_1(\omega)_{max}$ (arb. unit)	6.516	7.028	7.426	7.562	7.716	7.419	7.755	7.761	8.064	8.100	8.151
Energy at $\varepsilon_1(\omega)_{max}$ eV	3.279	3.388	3.415	3.325	3.279	3.306	3.388	3.388	3.306	3.143	3.061
$\varepsilon_1(\omega)_{min}$	-1.328	-1.266	-1.180	-1.120	-1.072	-1.091	-0.980	-0.896	-0.806	-0.831	-0.921
Energy at $\varepsilon_1(\omega)_{min}$ eV	6.381	6.408	6.599	6.581	6.599	6.190	6.245	6.327	6.327	6.272	6.435
$\varepsilon_2(\omega)_{max}$ (arb. unit)	6.687	7.166	7.311	7.571	7.889	7.592	7.550	7.572	7.938	7.994	7.909
Energy at $\varepsilon_2(\omega)_{max}$ eV	4.313	4.313	4.286	4.107	4.095	3.959	4.177	4.095	3.905	3.850	3.932
$\varepsilon_2(\omega)$ energy threshold (eV)	1.864	1.973	1.837	1.800	1.755	1.510	1.674	1.591	1.483	1.319	1.564
$n(0)$ (arb. unit)	1.942	1.942	1.953	1.962	1.970	2.015	1.975	1.987	2.010	2.043	2.073
$n(\omega)_{max}$ (arb. unit)	2.622	2.715	2.802	2.821	2.875	2.833	2.877	2.890	2.947	2.941	2.870
Energy at $n(\omega)_{max}$ eV	3.822	3.442	3.442	3.401	2.524	3.361	3.415	3.415	3.333	3.170	3.333
$k(\omega)_{max}$ (arb. unit)	1.588	1.602	1.658	1.691	1.739	1.700	1.724	1.732	1.746	1.822	1.785
Energy at $k(\omega)_{max}$ eV	6.245	4.395	4.367	4.351	4.340	4.204	4.340	4.231	4.095	4.041	4.013
$k(\omega)$ energy threshold (eV)	2.571	2.563	2.571	2.476	2.475	2.163	2.415	2.314	2.365	2.000	1.755
$\sigma(\omega)_{max}$ $(\Omega^{-1}cm^{-2})$	3.560	3.747	3.788	3.821	3.922	3.647	3.814	3.761	3.773	3.750	3.770
Energy at $\sigma(\omega)_{max}$ eV	5.401	4.340	4.286	4.192	4.122	4.013	4.201	4.122	3.959	3.905	3.959
$\sigma(\omega)$ energy threshold (eV)	2.490	2.571	2.490	2.461	2.408	2.136	2.354	2.255	2.163	1.973	1.855
$R(0)$ (arb. unit)	0.103	0.103	0.104	0.106	0.107	0.113	0.107	0.109	0.113	0.117	0.122
$R(\omega)_{max}$ (arb. unit)	0.369	0.365	0.359	0.352	0.346	0.346	0.332	0.333	0.337	0.351	0.346
Energy at $R(\omega)_{max}$ eV	6.735	6.789	6.653	6.638	6.626	6.472	4.340	4.215	4.030	4.068	4.014

REFERENCES:

Chad Husko, Joohoon Kang, Gregory Moille, Joshua D. Wood, Zheng Han, David Gosztola, Xuedan Ma, Sylvain Combrié, Alfredo De Rossi, Mark C. Hersam, Xavier Checoury, and Jeffrey R. Guest, (2018), **Silicon-Phosphorene Nanocavity-Enhanced Optical Emission at Telecommunications Wavelengths**, NanoLetters,18 (10), 6515-6520; DOI: 10.1021/acs.nanlett.8b03037.

Xiaojie Duan and Charles M. Lieber, (2015), **Nanoscience and the Nano-Bioelectronics Frontier**. Nano Research, 8, 1-22.

Peidong Yang, Ruoxue Yan and Melissa Fardy. (2010), **Semiconductor Nanowire: What's Next?** Nano Letters, 10(5), 1529-1536.

Xing Dai, Sen Zhang, Zilong Wang, Giorgio Adamo, Hai Liu, Yizhong Huang, Christophe Couteau, and Cesare Soci.(2014) **GaAs/AlGaAs Nanowire Photodetector**. Nano Letters, 14, 2688-2693.

Habeom Lee, Wanit Manorotkul, Jinhwan Lee, Jinhyeong Kwon, Young Duk Suh, Dongwoo Paeng, Costas P. Grigoropoulos, Seungyong Han, Sukjoon Hong, Junyeob Yeo, and Seung Hwan Ko. (2017), **Nanowire-on-Nanowire: All-Nanowire Electronics by On-Demand Selective Integration of Hierarchical Heterogeneous Nanowires**. ACS Nano, 11, 12311-12317.

Muskens O. L., J. G. Rivas, R. E. Algra, E. P. A. M. Bakkers, and A. Lagendijk. (2008), **Design of Light Scattering in Nanowire Materi-als for Photovoltaic Applications**. Nano Letters, 8(9), 2638-2642; DOI: 10.1021/nl0808076.

Muskens O. L., S. L. Diedenhofen, B. C. Kaas, R. E. Algra, E. P. A. M. Bakkers, J. G. Rivas, and A. Lagendijk. (2009), **Large Photonic Strength of Highly Tunable Resonant Nanowire Materials.** Nano Letters, 9(3), 930-934; DOI: 10.1021/nl802580r

Ochoa-Martínez E., L. Barrutia, M. Ochoa, E. Barrigón, I. García, I. Rey-Stolle, C. Algora, P. Basa, G. Kronome, M. Gabás. (2018), **Refrac-tive indexes and extinction coefficients of n- and p-type doped GaInP, AlInP and AlGaInP for multijunction solar cells**. Solar Energy Materials and Solar Cells, 174, 388-396; DOI: 10.1016/j.solmat.2017.09.028

Yamaguchi, M. (2003), III–V compound multi-junction solar cells: present and future, Solar Energy Materials and Solar Cells 75(1-2), 261–269.; DOI: 10.1016/S0927-0248(02)00168-X.

Kang D., W. Park, B. Kim, J. Kim, and C. Lee. S. l.(2004), **Change in electrical characteristics of gallium phosphide nanowire transistors under different environments**, 4th IEEE Conference on Nanotechnology, 2004., Munich, Germany, 2004, pp. 370-372, doi: 10.1109/NANO.2004.1392354.

Long Y., Z. Chen, W. Wang, F. Bai, A. Zin, and C. Gu. S. l. (2005), **Electrical conductivity of single CdS nanowire synthesized by aqueous chemical growth**. Applied Physics Letters, 86(15), 153102.; DOI: 10.1063/1.1900950.

Zeng H., M. Zheng, R. Skomski, D. J. Sellmyer, Y. Liu, Menon, L., and Bandyopadhyay, S. s.l.(2000), **Magnetic properties of self-assembled Co nanowires of varying length and diameter**. Journal of Applied Physics, 87(9), 4718-4720.; DOI: 10.1063/1.373137.

Deyu Li, Yiying Wu, Philip Kim, Li Shi, Peidong Yang et al. s.l.(2003), **Thermal conductivity of individual silicon nanowires.** Ap-plied Physics Letters, 83(14), 2934-2936.; DOI: 10.1063/1.1616981.

A'lvaro S. P., Noel Arellano, Jose A. Plaza, Rongrui He, Carlo Carraro, Roya Maboudian, Roger T. Howe, Jeff Bokor, and Peidong Yang. (2007), **Suspended Mechanical Structures Based on Elastic Silicon Nanowire Arrays**. Nano Letters, 7, 1100-1104.; DOI: 10.1021/nl062877n

Tong L., Jingyi Lou, and Eric Mazur. (2004), **Single-mode guiding properties of subwavelength-diameter silica and silicon wire waveguides** Optical Express, 12(6), 1025-1035.;DOI: 10.1364/OPEX.12.001025

Tong L., Gattass RR, Ashcom JB, He S, Lou J, Shen M, Maxwell I, Mazur E. Nature, 426, 816-819(2003).

Khordad R. and H. Bahramiyan,(2015), **Absorption threshold frequency of silicon nanowires: Effect of cross section shape**. Opt. Commun. 334, 85-89.;DOI: 10.1016/j.optcom.2014.08.025.

Yao, D., Zhang, G., Lo, G.-Q., & Li, B. (2009). **Impacts of size and cross-sectional shape on surface lattice constant and electron effective mass of silicon nanowires.** Applied Physics Letters, 94(11), 113113. doi:10.1063/1.3103366.

Vashaee, D., Shakouri, A., Goldberger, J., Kuykendall, T., Pauzauskie, P., & Yang, P. (2006). **Electrostatics of nanowire transistors with triangular cross sections**. Journal of Applied Physics, 99(5), 054310. doi:10.1063/1.2168229.

Gradečak, S., Qian, F., Li, Y., Park, H.-G., & Lieber, C. M. (2005**). GaN nanowire lasers with low lasing thresholds.** Applied Physics Letters, 87(17), 173111.; DOI:10.1063/1.2115087.

Borghesi A., G. Guizzetti. Gallium Phosphide (GaP), **Handbook of Optical Constants of Solids.** (London: Academic Press, 1991), page 445-464. Vol. I.

McIntosh D., Qiugui Zhou, Yaojia Chen, and Joe C. Campbell,(2011), **High quantum efficiency GaP avalanche photodiodes,** Optics. Express, 19(20),19607-19612. DOI:10.1364/oe.19.019607

Vaisman, M., Tomasulo, S., Masuda, T., Lang, J. R., Faucher, J., & Lee, M. L. (2015). **Effects of growth temperature and device structure on GaP solar cells grown by molecular beam epitaxy**. Applied Physics Letters, 106(6), 063903. DOI:10.1063/1.4908181.

Lang, J. R., Faucher, J., Tomasulo, S., Nay Yaung, K., & Larry Lee, M. (2013). **Comparison of GaAsP solar cells on GaP and GaP/Si.** Applied Physics Letters, 103(9), 092102. DOI:10.1063/1.4819456

Mohammad, R., & Katırcıoğlu, Ş. (2019). **Structural stability and electronic properties of different cross-sectional unstrained and rectangular cross-sectional strained GaP nanowires.** International Journal of Modern Physics B, 1950006. DOI:10.1142/s0217979219500061 .

Lin G., Q. Zhang, X. Lin, D. Zhao, R. Jia, N. Gao, Z. Zuo, X. Xu and D. Liu. (2015). **Enhanced photoluminescence of gallium phosphide by surface plasmon resonances of metallic nanoparticles.** RSC Advances, 5(60), 48275-48280.; DOI: 10.1039/C5RA07368E.

Sanatinia R., Marcin Swillo, and Srinivasan Anand.(2012). (2012). **Surface Second-Harmonic Generation from Vertical GaP Nanopillars**. Nano Letters, 12(2), 820–826. doi:10.1021/nl203866y.

Hwang S.Y., T.J. Kim, Y.W. Jung, N.S. Barange, H.G. Park, J.Y. Kim, Y.R. Kang, Y.D. Kim, S.H. Shin, J.D. Song, C.-T. Liang, Y.-C. Chang.(2014). **Dielectric function and critical points of AlP determined by spectroscopic ellipsometry.** Journal of Alloys and Compounds, 587, 361-364.; DOI: 10.1016/j.jallcom.2013.10.205

Kumar, V and Singh, J K. Kumar.(2010), **Model for calculating the refractive index of different materials**. Indian Journal of Pure and Applied Physics 48(8), 571-574.

Kim T.J. and S.Y. Hwang and J.S. Byun and D.E. Aspnes and E.H. Lee and J.D. Song and C.-T. Liang and Y.-C. Chang and H.G. Park and J. Choi and J.Y. Kim and Y.R. Kang and J.C. Park and Y.D. Kim,(2014). **Dielectric functions and interband transitions of InxAl1 − xP alloys.** Current Applied Physics, Volume 14, Issue 9,1273-1276.; DOI: 10.1016/j.cap.2014.06.026

Allali D., A. Bouhemadou, E. Muhammad Abud Al Safi, S. Bin-Omran, M. Chegaar, R. Khenata, A.H. Reshak.(2014), **Electronic and optical properties of the SiB2O4 (B=Mg, Zn, and Cd) spinel oxides: An ab initio study with the Tran–Blaha-modified Becke–Johnson density functional.** Physica B: Condense Matter, 443, 24-34.;DOI: 10.1016/j.physb.2014.02.053

Logothetidis, S. and Petalas, J. and Cardona, M. and Moustakas, T. D.,(1994), **Optical properties and temperature dependence of the interband transitions of cubic and hexagonal GaN**. Phys. Rev. B, 50,18017-18029.; DOI: 10.1103/PhysRevB.50.18017

Anani M., C. Mathieu, S. Lebid, Y. Amar, Z. Chama, H. Abid.(2008), Model for **Calculating the Refractive Index of a III-V Semi-conductor**. Computational Materials Science, 41, 570-575.; DOI: 10.1016/j.commatsci.2007.05.023

Claudia Ambrosch-Draxl, Jorge O. Sofo,(2006), **Linear optical properties of solids within the full-potential linearized augmented planewave method** Computer PhysicsCommunications,175,1-14.;DOI: 10.1016/j.cpc.2006.03.005

Aspnes D. E. and A. A. Studna,(1983), **Dielectric functions and optical parameters of Si, Ge, GaP, GaAs, GaSb, InP, InAs, and InSb from 1.5 to 6.0 eV**, Phys. Rev. B, 27, 985.

Moussa R., and A. Abdiche and R Khenata and D P Rai and W K Ahmed and S Bin Omran and G Murtaza and F Soyalp,(2015), **Studying structural, electronic and optical properties of zinc-blende Ga1−xAlxP at normal and under pressure by means of first principle**. Materials Research Express, 2,105904. DOI: 10.1088/2053-1591/2/10/105904.

Saadi Berr,(2017) **Theoritical analysis of the structural, electronic and optical properties of tetragonal Sr2GaSbO6.** Chinese Journal of Physics, 55,2476-2483. Doi: 10.1016/j.cjph.2017.11.001

Blaha P., K. Schwarz, G.K.H. Madsen, D. Kvasnicka, J. Luitz, WIEN2k, An Augmented-Plane-Wave+Local Orbitals Program for Calcu-lating Crystal Properties, Karlheinz Schwarz, Techn. Universitat, Wien, Austria, 2001, ISBN 3-9501031-1-2.